Tectonophysics 860 (2023) 229919

Contents lists available at ScienceDirect

Tectonophysics

journal homepage: www.elsevier.com/locate/tecto

Nature and origin of an undetected seismic phase in waveforms from Southern Tyrrhenian (Italy) intermediate-depth and deep earthquakes: first evidence for the phase-A in the subducted uppermost lithospheric mantle?

Teresa Ninivaggi [a,*], Giulio Selvaggi [b], Salvatore Mazza [b], Marilena Filippucci [b,c], Fabrizio Tursi [d], Wojciech Czuba [e]

[a] Istituto Nazionale di Geofisica e Vulcanologia, Sezione Irpinia, C. da Ciavolone, 83035 Grottaminarda, AV, Italy
[b] Istituto Nazionale di Geofisica e Vulcanologia, Via di Vigna Murata, 605, 00143 Roma, RM, Italy
[c] Università degli Studi di Bari "Aldo Moro", Dipartimento di Scienze della Terra e Geo-ambientali, Via Orabona, 4, 70125 Bari, BA, Italy
[d] Università degli Studi di Torino, Dipartimento di Scienze della Terra, Via V. Caluso, 35, 10125 Torino, TO, Italy
[e] Institute of Geophysics, Polish Academy of Sciences, 64 Księcia Janusza Str., 01-452 Warsaw, Poland

ARTICLE INFO

Keywords:
Later seismic arrival/phase
Waveforms analyses
Intermediate and deep seismicity
Southern Tyrrhenian subduction zone
Mineral phase A

ABSTRACT

We have found a previously unreported later seismic phase in seismograms of European seismic stations from intermediate-depth and deep earthquakes of the Southern Tyrrhenian subduction zone. We observe this phase at stations from 6 to 9° from the epicentre, towards north. Only seismograms of earthquakes located in a well-defined region of the slab, in the depth range of 215–320 km, show the later *x*-phase. In this work, we describe the nature and possible origin of this phase, and we provide a simple 2D model to explain the observed arrival times. Our analyses reveal that the *x*-phase propagates downward in a high velocity layer, possibly located within the deepest part of the slab. We suggest that this layer reveals the presence of the dense hydrous magnesium silicate *phase A*, introduced from petrological laboratory experiments, inferred to carry water in the upper mantle and predicted to be found in cold subduction zones.

1. Introduction

Seismograms of deep earthquakes from many subduction zones show later phases. Most of these observations come from the Pacific subduction zones and they have been widely used to get useful indication on the geometric characteristics of subducting slabs (Hasegawa et al., 1978; Matsuzawa et al., 1986; Ohmi and Hori, 2000; Zhao et al., 1997). These phases are generally associated to *P (S)* waves converted or reflected at the upper slab interface from the direct *S (P)* waves (Ohmi and Hori, 2000; Zhao, 2019; Zhao et al., 1997; Fukao et al., 1978; Obara and Sato, 1988). Waves traveling upwards from the hypocentre and reflected at the surface at the bouncing point near the epicentre are called *depth phases* and they are traditionally exploited to constrain hypocentral depths (e.g., Zhao, 2019). Later phases could be also ascribed to *S*-wave reflections from a magma reservoir observed on crustal earthquakes, in addition to *S*-shadows waves observed on deep earthquakes and at particular azimuths (Lin, 2016; Lin et al., 2018). Observations of dispersive and complicated wave trains are also relevant in seismograms of deep earthquakes as they provide important implications for the petrological properties of subducted lithosphere. For example, dispersive high frequency trains of *P*- and *S*-waves observed at the fore-arc seismic stations of the Hellenic Trench from intermediate depth earthquakes reveal the presence of a low velocity channel in the upper part of the slab (Abers, 2000, 2005; Essen et al., 2009; Hori, 1990; Martin et al., 2003; Martin and Rietbrock, 2006). The low velocity channel is an important finding to trace water path within the subduction process. High frequency guided waves have been also described for the Japanese subduction and Northwestern Pacific subductions. They are interpreted as scattered seismic waves by heterogeneity in plate structure (Furumura and Kennett, 2005; Furumura and Kennett, 2021; Kennett and Furumura, 2013; Kennett and Furumura, 2015). This effect could be enhanced by a metastable olivine wedge (Furumura et al., 2016). Similar characteristics were also found in seismograms of Calabria stations, recorded from deep earthquakes of the Southern Tyrrhenian

* Corresponding author at: Istituto Nazionale di Geofisica e Vulcanologia, sede di Milano, Via Alfonso Corti, 12, 20133 Milano, MI, Italy.
E-mail addresses: teresa.ninivaggi@ingv.it (T. Ninivaggi), giulio.selvaggi@ingv.it (G. Selvaggi), salvatore.mazza@ingv.it (S. Mazza), marilena.filippucci@uniba.it (M. Filippucci), fabrizio.tursi@unito.it (F. Tursi), wojt@igf.edu.pl (W. Czuba).

https://doi.org/10.1016/j.tecto.2023.229919
Received 20 September 2022; Received in revised form 11 May 2023; Accepted 15 May 2023
Available online 24 May 2023

subduction zone (Sun et al., 2014).

Working on seismograms of a deep earthquake from the Southern Tyrrhenian subduction zone occurred in 2011, we noticed a clear later phase, few seconds after the direct *P*-wave, at stations located some hundreds of km away from the epicentre towards north (Fig. 1).

This phase, that we have called *x*-phase, disappears at stations located in central and northern Europe (Fig. 2). In a first stage of the work, we accepted the same lines of interpretation of the quoted literature, but we soon understood that the arrival times of the phase we were looking at were not consistent neither with a sP (pS) converted phase, nor with a guided wave. This because the lag times after direct arrivals are constant for converted waves at the upper plate boundary of the subducting slab (Zhao et al., 1997) or increase with distance for guided waves in the oceanic crust (Hori, 1990). The difference in arrival times between our phase and the direct *P*-wave decreases with the epicentral distance and it does in a way that excludes such interpretations.

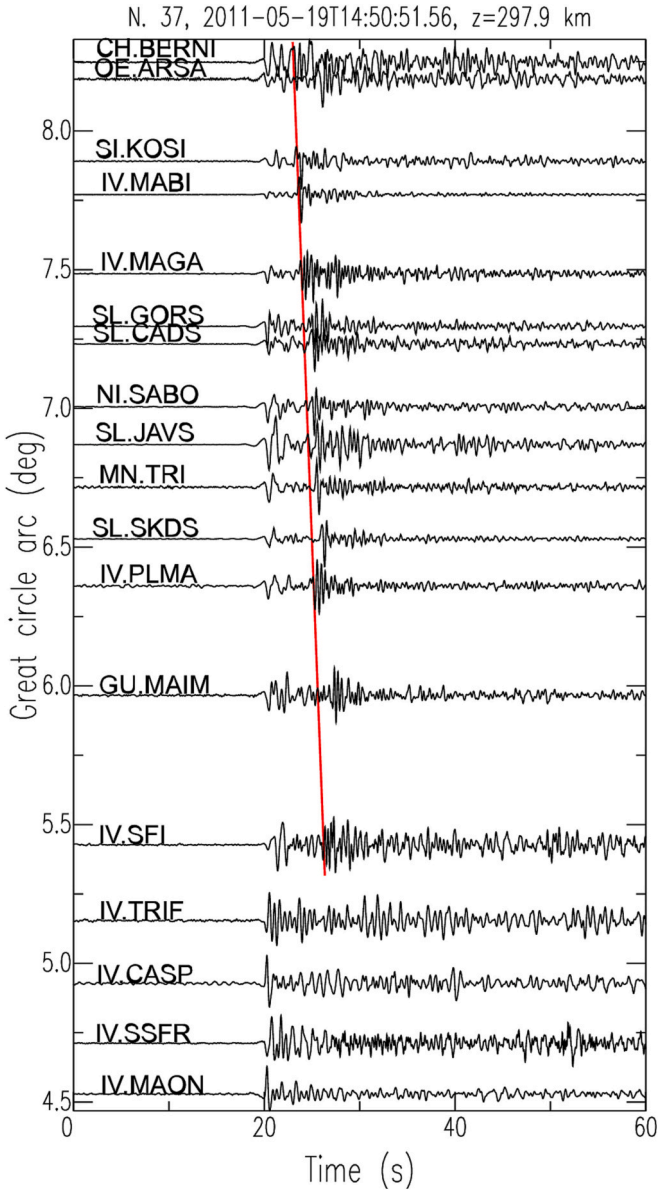

Fig. 1. Time-distance vertical seismograms of the 2011 event aligned with P arrival time at 20 s. The red line marks the later phase arrivals. (For interpretation of the references to colour in this figure legend, the reader is referred to the web version of this article.)

We decided, then, to investigate a wider dataset composed of the 43 deep and largest earthquakes of the Southern Tyrrhenian subduction zone and to perform waveforms analyses to derive the main seismological features of the unreported phase. We, finally, made a 2D ray path modelling to infer the origin of the *x*-phase. In this paper, we first describe the dataset and the observations related to the seismic phase then, we use the results to constrain a 2D model of the slab to explain the observations. One major point we discuss in this work is the possible identification in the subducting slab of a dense magnesium silicate mineral phase carrying water in the upper mantle and the petrological implication of this finding.

2. Tectonic setting

The Southern Tyrrhenian basin is the result of the Ionian lithosphere rollback and associated opening of the back arc basin that lasted for 80 Myr (Faccenna et al., 2001). Based on tomographic images, plate tectonics reconstructions and geological data, Faccenna et al. (2001) recognised multiple evolutionary stages of the subduction process characterised by different back-arc opening rates, sometimes as fast as 30–40 mm/yr (Fig. 2). The slab should have reached the 660 km transition zone after about 60–70 Myr of subduction process (Faccenna et al., 2001). GNSS velocity field (D'Agostino et al., 2011) shows that the present day roll back, if any, of the Ionian lithosphere could be at the level of 1 mm/yr, much slower than in the past. The subduction of the Ionian lithosphere beneath the Calabrian arc and the Tyrrhenian Sea is nowadays marked by an intense intermediate and deep seismicity. The occurrence of deep earthquakes beneath the Southern Tyrrhenian Sea has been well known since the seventies, and reported in a wide literature (Ritsema, 1972; see also Chiarabba et al., 2008; Scarfì et al., 2018; Selvaggi and Chiarabba, 1995). The seismicity distribution clearly defines a NW-dipping Wadati-Benioff plane from the Ionian Sea towards the central Tyrrhenian Sea. Earthquakes can be as deep as 600 km (Fig. 3). Seismicity distribution and tomographic images show that the descending Ionian slab is very steep (~70°) in the first 300–350 km and starts flattening below those depths (Chiarabba et al., 2008; Cimini and Marchetti, 2006; Lucente et al., 1999; Scarfì et al., 2018; Spakman et al., 1993).

The slab is seismically continuous only in its southwestern part, beneath the Aeolian Islands (Fig. 3b) while, in the north-eastern portion, along the Calabrian coasts, the slab is mostly aseismic between 100 km and 250 km depth (Fig. 3c). The aseismic part of the slab has been interpreted as an indication that the slab is dying out along a horizontal break-off that propagates in a scissor-type mode (Amato et al., 1993; Scarfì et al., 2018; Spakman et al., 1993).

The Southern Tyrrhenian slab is in down dip shortening in a large part of it, from about 100 km down to 400 km depth, and the magnitude of earthquakes increases with depth (Frepoli et al., 1996; Selvaggi, 2001). The largest earthquake occurred in 1938 and had a magnitude of 7.1 (Anderson and Jackson, 1987). The depth estimate was 290 km, and it is one of the largest earthquakes ever recorded in Italy. The way the slab deforms suggests that the gravitational pull is probably the main driving force of the subduction.

3. Data and Methods

We decided to make a systematic analysis of intermediate depth and deep earthquakes from the Tyrrhenian subduction zone to further investigate and constrain the previous observations on the *x*-phase. We selected the 43 largest earthquakes from 1990 to 2020 ($M_L \geq 4.5$) located in Southern Tyrrhenian region from the INGV Italian Seismological Instrumental and Parametric Database (http://cnt.rm.ingv.it/iside). The depth range is between 100 km and 644 km. The list of earthquakes and additional examples of the computed analysis from the whole dataset are available in the supplementary material.

We extracted the digital waveforms of the earthquakes from the

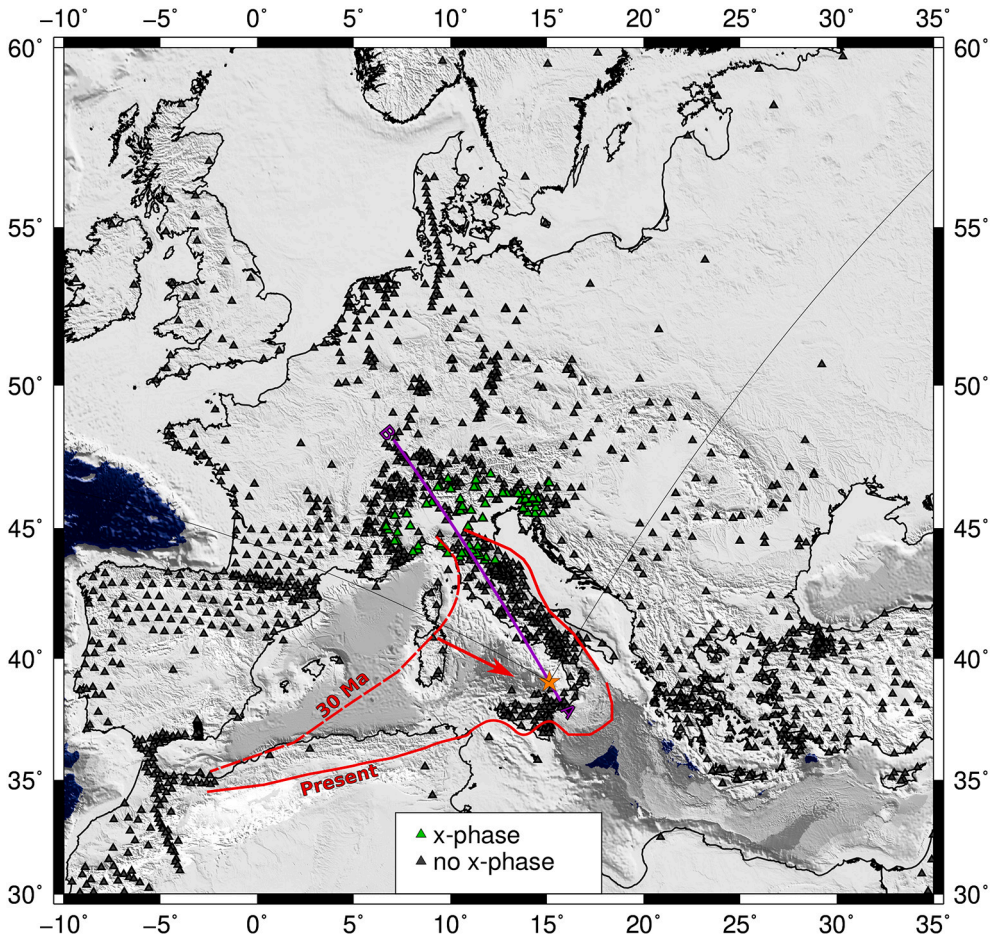

Fig. 2. Stations which recorded the x-phase (green triangles). Seismograms of stations in black do not show the later arrival. Section trace AB of the Fig. 9, passing from the 2011 earthquake (n. 37). The red lines delineate the old (30 Ma) and the present subduction signature. The two thin black lines delineate the azimuths −60° and 30° starting from the epicentre. (For interpretation of the references to colour in this figure legend, the reader is referred to the web version of this article.)

European Integrated Data Archive, 2023 (EIDA, http://eida.ingv.it/) and from Incorporated Research Institutions for Seismology Data Management Centre, 2023 (IRIS DMC, https://service.iris.edu/). The selected seismic stations are from 10° up to 71° North in latitude (from Central Africa to north Norway) and between 10° West and 50° East in longitude (from Portugal to eastern Turkey). We used seismograms from broadband high gain seismometers (HH or BH streams) for each earthquake, when available. If they were not, we used short period high gain seismometers (EH or SH), especially for the oldest earthquakes. To analyse the whole dataset, i.e., >25,000 seismograms, we plot record sections normalising each waveform by its absolute maximum amplitude, excluding the *S*-waves from the plot windows. We sorted seismograms by increasing source-receiver distance and aligned by direct *P,* manually picked, arrival time. Phase recognition in the selected dataset was made through visual inspection on the record sections. Record sections for the whole dataset were analysed dividing the large number of stations in angular sectors of about 45 to 60 degrees of azimuth. Fig. 4 shows an example of a record section for two different azimuths. We generally observe the *x*-phase along the direction perpendicular to the slab surface (Fig. 4a) from 600 to about 1000 km from the epicentre and in the range from −60 to 30°. For the complementary sector, from 30 to 300° clockwise, record sections never show the *x*-phase (Fig. 4b).

The *x*-phase is rather prominent and easy to recognise. It often appears in the vertical component as an impulsive arrival with an amplitude about two times larger than the first *P*-arrival (Fig. 5a). It is also clearly visible in the horizontal component and again it has a larger amplitude with respect to the direct *P* wave. The *x*-phase has similar amplitude on the vertical and radial component, and both are about the double with respect to the transverse component.

At greater distances, from 11° onwards, we found another arrival after the direct *P*-wave that is well reproduced by the 410 km discontinuity (P410P in the Fig. 4).

We also noticed that the *x*-phase has, generally, a higher frequency content in comparison to the direct *P*-wave. The station MABI in Fig. 5b shows, for example, a peak in the power spectra at about 1–2 Hz, instead the *x*-phase has a higher frequency content than *P*, up to 4 Hz. We did not perform systematic analyses on the frequency content as it is not the goal of this paper, and it will be part of a future work.

4. Results

The diagrams in Fig. 6 shows the particle motion and the incidence angle of the first *P*-arrival and the later *x*-phase at SOKA station located 7.9° away from the epicentre. The selected earthquake occurred at a depth of 255 km beneath the Aeolian Islands. The ray-path for both phases is linear and mainly oriented in the radial direction which is the source-receiver back-azimuth direction (Fig. 6 b-c). The *x*-phase shows a typical *P*-wave particle motion, and we verified that this is a general observation for the *x*-phase. The incidence angle of the *x*-phase is always greater than the direct *P* (Fig. 6 d-e), These characteristics indicate that the *x*-phase is a compressional *P*-wave that travels in a less attenuating medium than the direct *P*-wave.

After analysing all the available record sections, we notice that the *x*-phase appears at about 6° from the epicentre, it is not present in all the

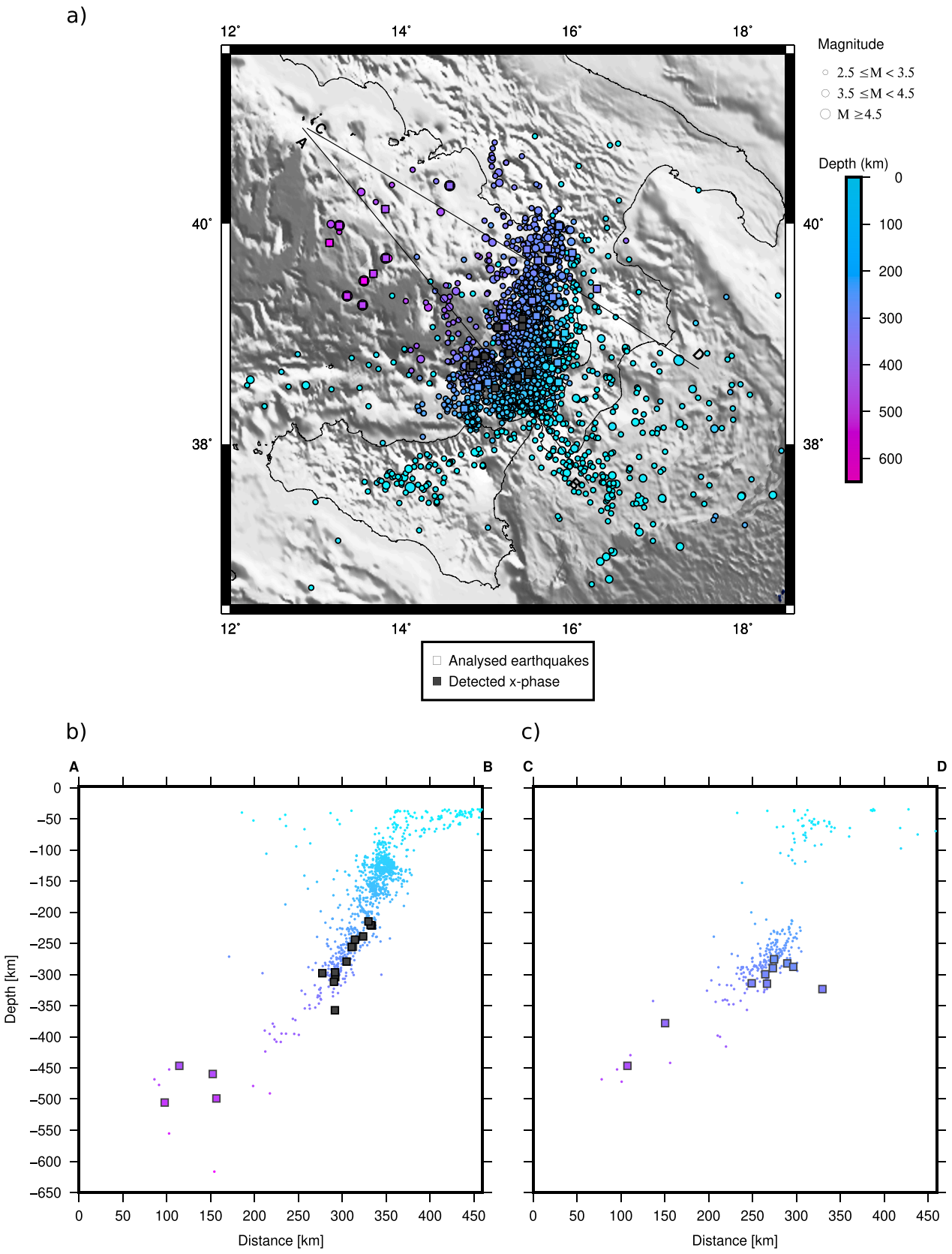

Fig. 3. Seismicity map of the Southern Tyrrhenian Subduction Zone from 1990 to 2020. (a) Squares are the 43 analysed earthquakes; grey filled squares are those earthquakes where we recognised the x-phase. (b) Vertical cross-sections perpendicular to the strike of the southwestern part of the slab (AB) and (c) its north-eastern part (CD).

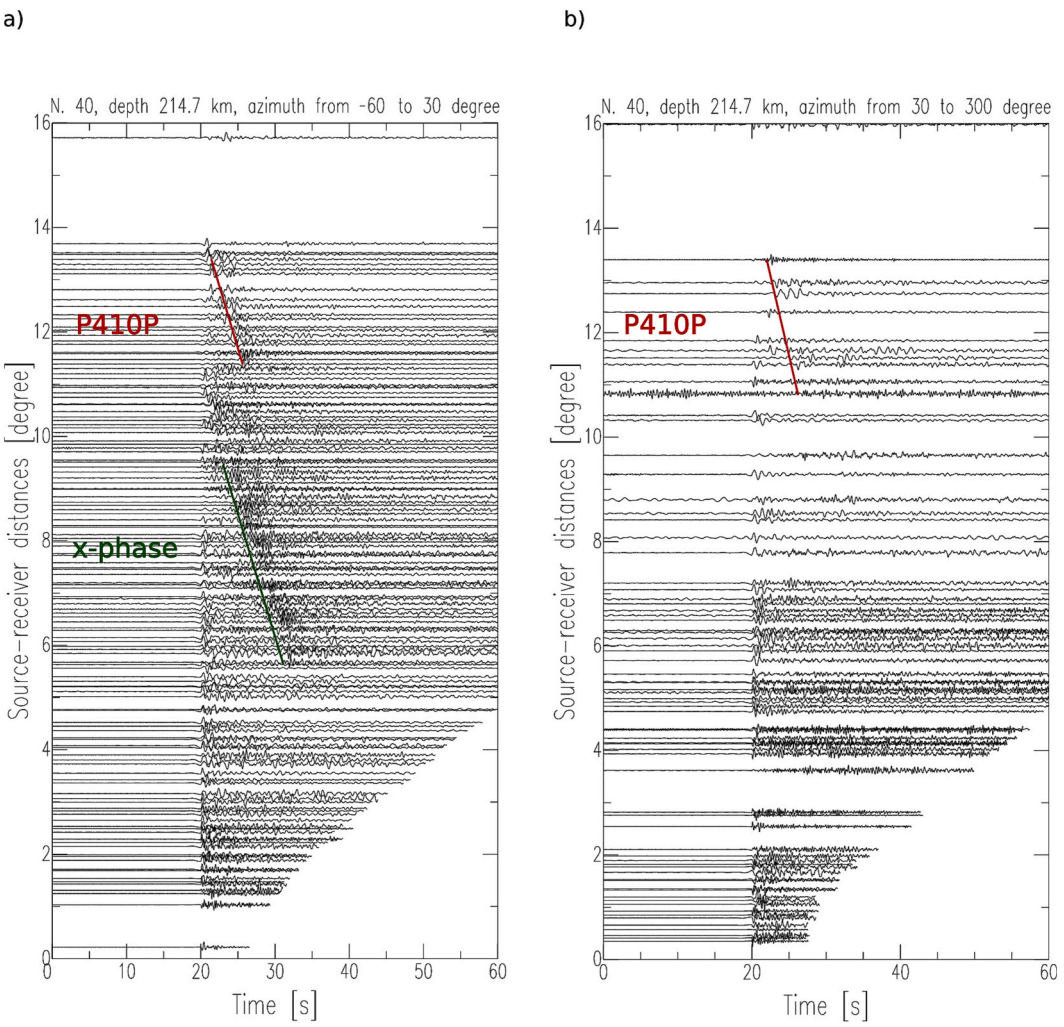

Fig. 4. (a) Record Section in the azimuth − 60÷30° for an intermediate depth earthquake of the Southern Tyrrhenian Subduction Zone. (b) Record Section for the same earthquake but for the complementary azimuth (30÷300°). The x-phase is visible only in the stations to the north of the epicentre at a distance from 600 km to about 1000 km.

events, and it is dependent on the azimuth. The time difference between direct *P* and the later wave, at the distance where the phase appears, is on average 10 s. The arrival time difference between the direct *P* and the *x*-phase decreases with epicentral distance and, at about 9°, *x*-phase merges with the direct-*P*.

The *x*-phase has an apparent velocity of about 11 km/s. Record sections show that the apparent velocity, after 9° and after the *x*-phase merges with the direct-*P,* is equal to the direct *P*-wave and not to that of the *x*-phase. This means that the *x*-phase reaches the surface only between 6 and 9° and not after or before these distances. This is a strong constraint in the *x*-phase interpretation. We then plot the seismograms in function of the foci depth for each station. The arrival time decreases with increasing depth at each station (Fig. 7). This suggests that the *x*-phase is in some way related with a deeper interface, probably within the slab. The deeper the earthquake, the shorter the difference in the arrival time between the direct *P*-wave and the *x*-phase (Fig. 7).

Arrival times indicate that the *x*-phase is not a depth phase. The main characteristic of depth phases is that the difference of arrival-time between a depth phase onset and the *P*-onset is an increasing function of the epicentral distance (Murphy and Barker, 2006). For the same reason, the *x*-phase is not even a *SP*-wave, which is a direct *S*-wave traveling upward and converted at the upper boundary of the slab, as analysed in Zhao et al. (1997) for the Japan slab. It has an apparent velocity almost equal or slightly smaller than the direct *P*-wave and the arrival time difference with the direct *P*-wave is constant. The *x*-phase is not a guided wave from the crust of the subducting lithosphere, being these waves characterised by apparent velocities smaller than first arrivals and comparable with oceanic crust or lower continental crust velocities (e.g., Hori, 1990). The *x*-phase is also dissimilar from guided waves described for the Northwestern subductions (e.g., Kennett and Furumura, 2013) as the latter have frequency content above 10 Hz, they are indistinguishable from first arrivals and are observed at distances >3000 km.

The later arrival, described in this work as the *x*-phase, is a *P*-wave that propagates downward interacting with the deepest portion of the subducted lithosphere.

Only seismograms of stations located in the northerly quadrants with respect to the epicentre show the later *P*-arrival, as shown in Figs. 2 and 4. Results can be generalised in the following way. All the seismograms between 6 and 9° from earthquakes with hypocentre below the Aeolian Arc and in the depth range 220 to 320 km show the *x*-phase, a compressional *P*-wave, as in the example of Fig. 8a. Earthquakes with hypocentre in the western side of Calabria's coasts never show the later phase, but only the phase associated to the ~410 km discontinuity (Fig. 8b). Earthquakes beneath the coast of Calabria occur in the same depth interval of the earthquakes beneath the Aeolian Islands. There are clear geometric differences between these two sectors of the slab and probably a combination of geometry of the slab and its velocity structure is a necessary condition to generate the later phase. Earthquakes with

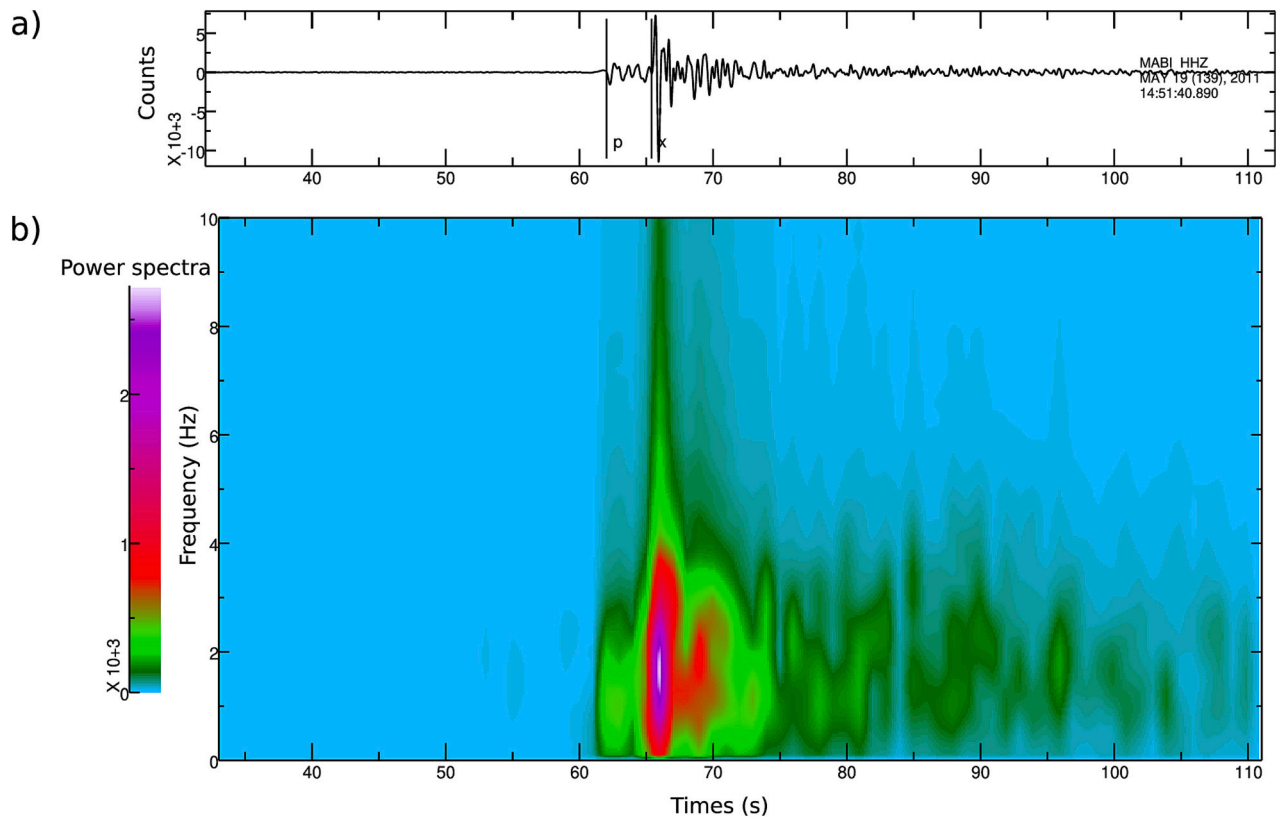

Fig. 5. Amplitude and frequency (a) Vertical waveform of station MABI located at 7.7° from epicentre; (b) spectrogram of the vertical component.

hypocentre deeper than 400 km do not show neither the later phase nor a phase associated to the 410 km discontinuity (Fig. 8c). Fig. 9 shows the spatial distribution of the three different cases. A further peculiar observation is from profile A–B of Fig. 3b. It shows that the earthquakes that show the *x*-phase have hypocentres below the Aeolian Islands and concentrate in the bottom part of the seismic zone. We compared two seismic catalogues (INGV Italian Seismological Instrumental and Parametric Database available at http://cnt.rm.ingv.it/iside and CLASS, Latorre et al., 2023) and the hypocentres, although slightly different, show the same pattern.

The seismological constraints derived from the observations made in this work, allow us to design a simple 2D modelling by means of fitting the arrival times. The final goal is to understand the nature and origin of the *x*-phase. We are aware that a 2D approach is a first approximation of a complex 3D geometry as it is the Southern Tyrrhenian subduction zone and future work will include a full 3D model to take into account the complex three-dimensional geometry of the problem.

We calculated theoretical travel time curves with Seis83 software (Červený and Pšenčík, 1984) that makes use of ray-tracing technique (Červený et al., 1977) with the graphical interface model (Komminaho, 1998) and ZPLOT (Zelt, 1994).

Several models were tested to match the arrival times of the *x*-phase. We used IASP91 velocity model (Kennett and Engdahl, 1991) to represent the velocity structure outside the slab (Fig. 10a), whereas the slab boundaries were constrained by seismicity distribution (Fig. 3b). Following Pino and Helmberger (1997), the 410-km discontinuity is raised up to a depth of 370 km, as generally observed in subduction zones (Collier et al., 2001). According to tomographic studies (Amato et al., 1993; Scarfì et al., 2018; Spakman et al., 1993), the subducting lithosphere is characterised by positive velocity anomalies. We increased the velocity inside the slab in different runs by a percentage between 1.5% and 5% to the IASP91 velocity values.

The arrivals of the direct *P*-wave are well fitted by a subducting lithosphere with an average increment of 1.5% of IASP91 velocity model, whereas the *x*-phase requires much faster velocities, at least 3% higher than IASP91. Hence, we introduced a high velocity layer, HVL, in the region where we observe the hypocentre of the earthquakes with the later phase with an average increase of the velocity up to 3% with respect to IASP91. Compressional velocities in the HVL between 250 and 370 km depth are from 8.9 to 9.15 km/s. The model is able to fit the arrival times of the *x*-phase for all the deep earthquakes below the Aeolian Island we have modelled (Fig. 10c).

The introduction of a HVL provides the explanation to most of the observations we have done in this work. It explains why the later phase is not observed in very deep earthquakes, below the 410 km discontinuity. It may explain also the different frequency content of the direct *P* wave if compared to that of the *x*-phase traveling along a different, probably less attenuating, path. It also provides an explanation why we see the *x*-phase only at specific epicentral distances (between 6 and 9°).

5. Discussion and Conclusions

We have described the nature and origin of a later arrival observed in intermediate-depth and deep earthquakes of the Tyrrhenian subduction zone at stations from 6 to 9° from epicentres, towards north. Only earthquakes beneath the Aeolian Islands and in the depth range between 215 and 320 km generate this later *P*-arrival. The 2D modelling shows that a combination of velocity structure and geometric characteristics is able to reproduce rather well the observations of the whole dataset.

The modelling procedure comes through many different models gradually improving the arrival times fit of the seismological observations we have made (observed *x*-phase arrival times and distances at which we observe the *x*-phase). The model is constrained by the well-known a priori tectonic information (e.g., seismicity distribution, geometric characteristics of the slab and available velocity models). All these a priori information limit the possibility to dramatically change the final model and the seismological observations we have shown in the manuscript are quite strong and drive in a “robust” way the possible

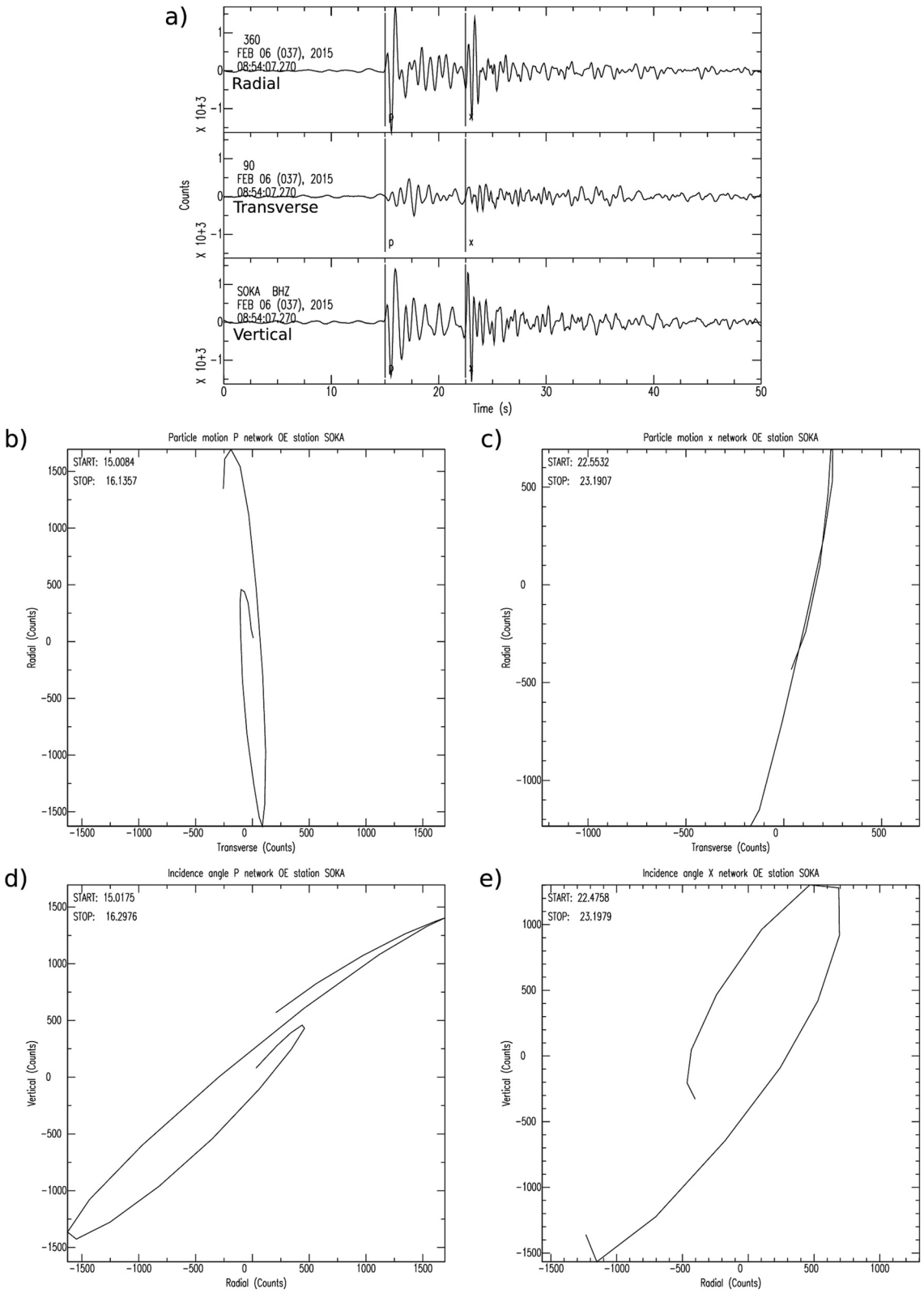

Fig. 6. Particle motion (a) Radial, transverse and vertical waveforms of station SOKA, located at 7.9° from the earthquake occurred on 2015-02-06 at 255 km of depth below the Aeolian Islands; (b) particle motion diagram of the direct P wave and (c) of the x-phase; (d) incidence angle of the direct P and (e) x-phase.

models. In particular, we observe that the arrival time difference between the direct P and the *x*-phase decreases as the epicentral distance and depth of the earthquake increases (see Fig. 7). This implies that the *x*-phase is a downward wave which leaves the source, travels in a higher velocity medium than direct P and interacts with an interface deeper than the hypocentre. The deepest earthquakes that show the *x*-phase are at ~320 km of depth. If there were a discontinuity at this depth (or thereabouts), the ray path of direct and *x*-phase would be similar, and it would be difficult to see differences in amplitude and frequency content between the two phases. Consequently, direct P and *x*-phase ray paths

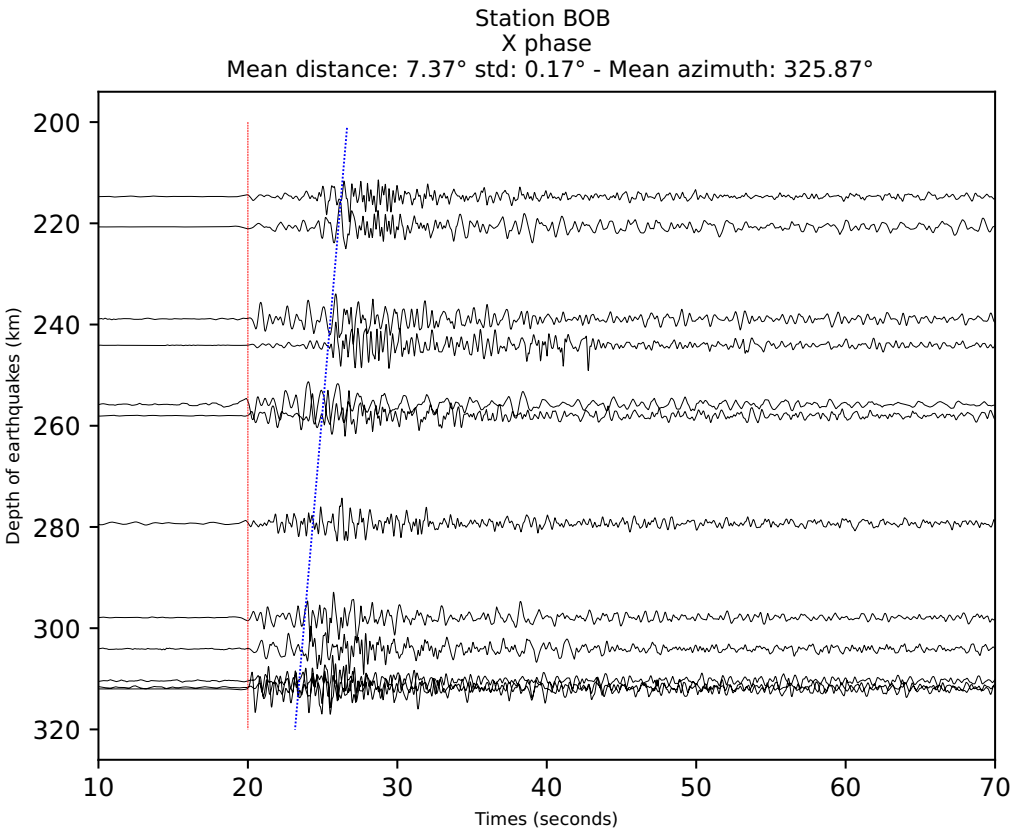

Fig. 7. Vertical waveforms recorded at the seismic station BOB for different earthquakes. They are sorted by earthquake depth and aligned by P first arrivals on the y-axis (the red vertical line). The blue line highlights the x-phase arrivals. (For interpretation of the references to colour in this figure legend, the reader is referred to the web version of this article.)

ought to be different and the discontinuity deep enough to ensure the right difference in the travel paths. Furthermore, a shallower discontinuity alone would not explain arrival times of the *x*-phase. We calculated arrival times and ray paths with the 1D velocity model of Pino and Helmberger (1997) computed for the West Mediterranean area. They found a discontinuity at 370 km of depth with a velocity contrast of 3% (same contrast of the 410 km – discontinuity in the iasp91 model). This model does not fit the arrival times of the *x*-phase and simultaneously the P410P phase. The latter is explained by a simple 1D model, with the discontinuity at 410 km, the former by higher velocity values at depths of 200–370 km.

This work shows kinematic determination of new *x*-phase without exact dynamic calculations. The velocity contrast is too low to generate so high amplitudes and it needs further investigations. More probably, the difference in amplitude and frequency content between direct *P* and *x*-phase could be due to an attenuated path followed by the direct wave.

Traveling upward, the *P* direct wave could cross the region where dehydration reactions and partial melting occur. Chiarabba et al. (2008) found a low Q_p anomaly and a high V_p/V_s ratio in the mantle wedge facing the slab, below the Aeolian Island, at depth between 150 and 250 km, revealing the fluid migration within the mantle. According to this hypothesis, the direct *P*-phase would travel in a higher attenuation medium compared to the medium crossed by the *x*-phase. This would explain why we have the *x*-phase with a higher amplitude and frequency content than the direct *P*.

As far as we know, a HVL, as the one we have introduced in this work, has not been previously described from a seismological point of view. The dubitative question mark in our title reflects some assumptions contained in the modelling and other considerations that should be verified. These refer to three main questions. Why tomographic images available for the Tyrrhenian subduction zone do not show such a HVL? Why the fast and late *P*-arrival has not been observed elsewhere, in other subduction systems? Are *P*-wave velocities as fast as 9.1 km/s reasonable at 300–350 km depth within a slab?

There are plenty of tomography results published for the Tyrrhenian subduction zone that use different datasets and inversion techniques (Amato et al., 1993; Chiarabba et al., 2008; Lucente et al., 1999; Selvaggi and Chiarabba, 1995; Spakman et al., 1993). None of them shows a clear well defined HVL, although all agree that at depths between 200 and 400 km, the *P*-velocity is higher than the velocity of the surrounding mantle but not at the level of the HVL we have introduced. An answer is that the thickness of the HVL could be as wide as 20–30 km and such layer is probably too narrow to be detected by the course grid generally used to model the mantle at those depths. The high velocities of the HVL could then be averaged within the general high *P*-velocity at those depths, masking the real velocity anomaly of the HVL. Nevertheless, we accept that the slab could be narrower than what is mapped by tomographic inversions (due to the resolution of the method and the uncertainties in earthquake locations). This does not affect the main conclusion that velocities as high as 9.1 traveling in a narrow slab or inside an HVL are needed.

The fact that we see the later *P*-arrival only in the Southern Tyrrhenian Subduction Zone, then, is probably due to the peculiar combination of the velocity structure, geometric conditions, as said before, as well as the station distribution in front of the slab. Concerning the Tyrrhenian subduction, we are particularly lucky as it has the whole Europe and its numerous seismological stations in front of it, spanning distances evenly for thousands of km. Such network geometry is not easy to find in other subduction zones. All the subductions along the Pacific have a less favourable network geometry. The distance between 6 and 9° from the epicentre for most of the pacific subductions are either in the sea or in less monitored areas. That is probably why the *x*-phase is not a

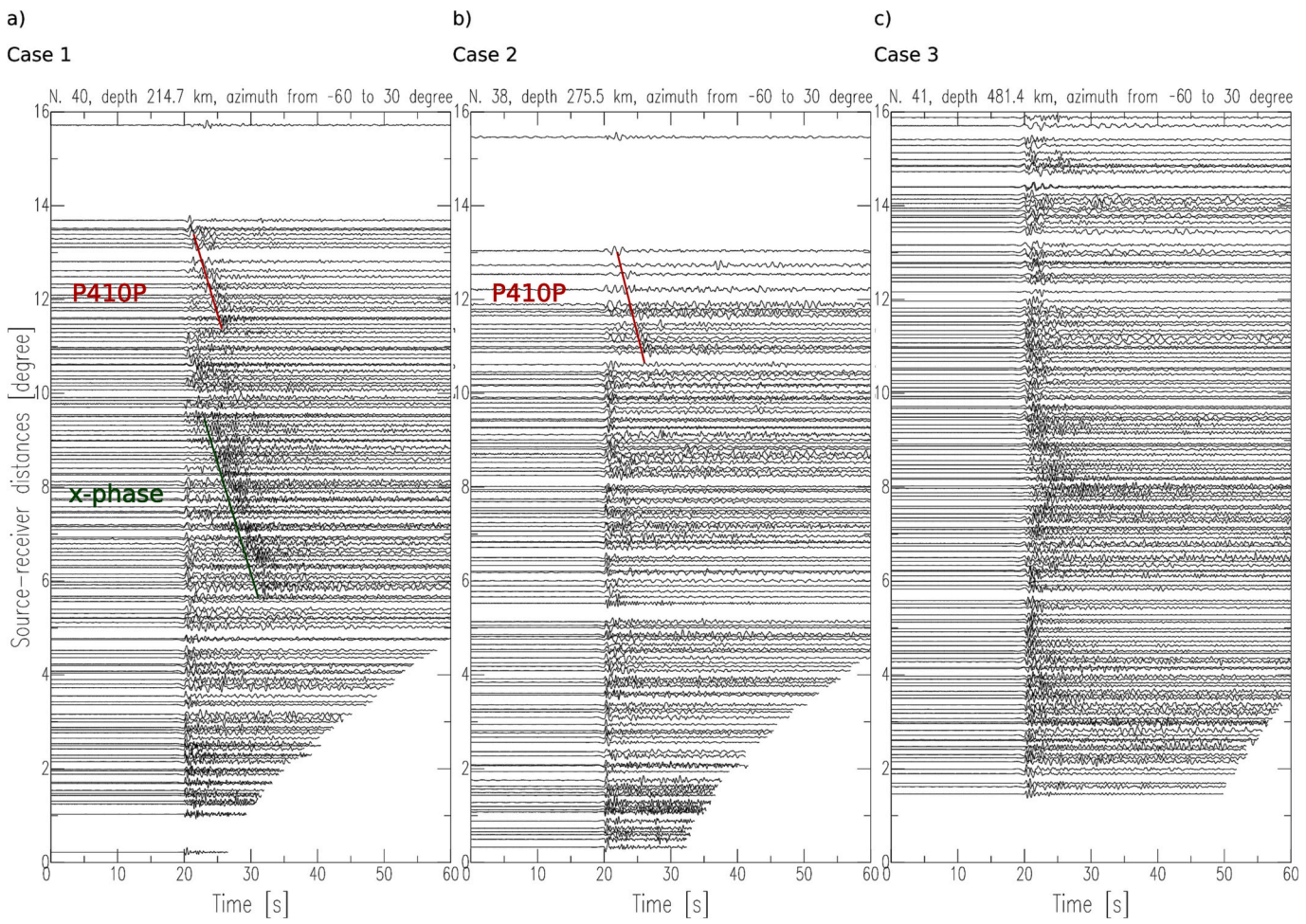

Fig. 8. Examples of record sections of the three cases we discuss in the text. The "N." in the title corresponds to number id in the map of the Fig. 8 (N. 40, 38, 41).

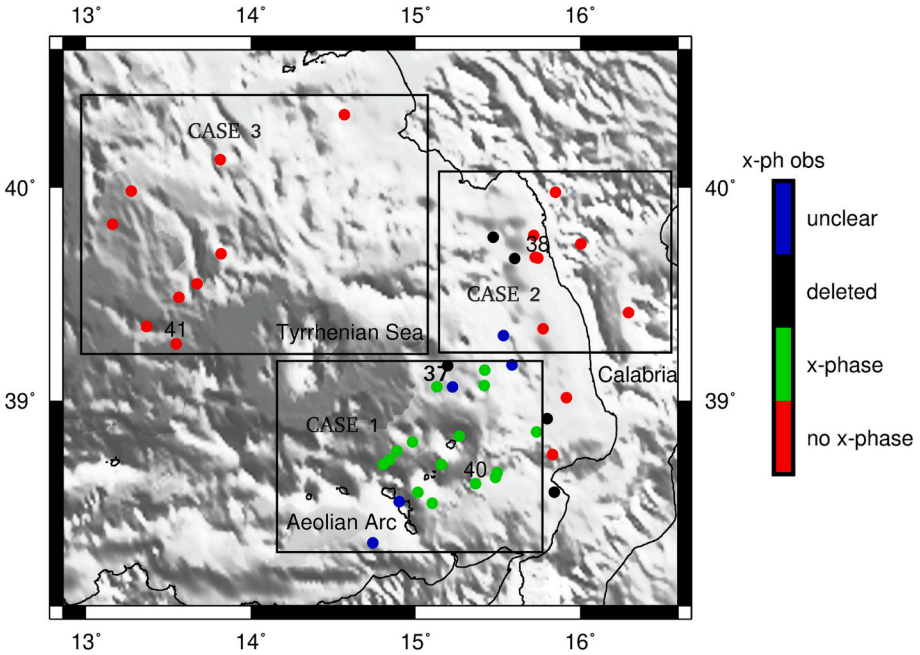

Fig. 9. Map distribution of the earthquakes that show the later seismic phase (green dots), that do not show the x-phase (red dots) and those earthquakes where the presence of the x-phase is unclear (blue dots). (For interpretation of the references to colour in this figure legend, the reader is referred to the web version of this article.)

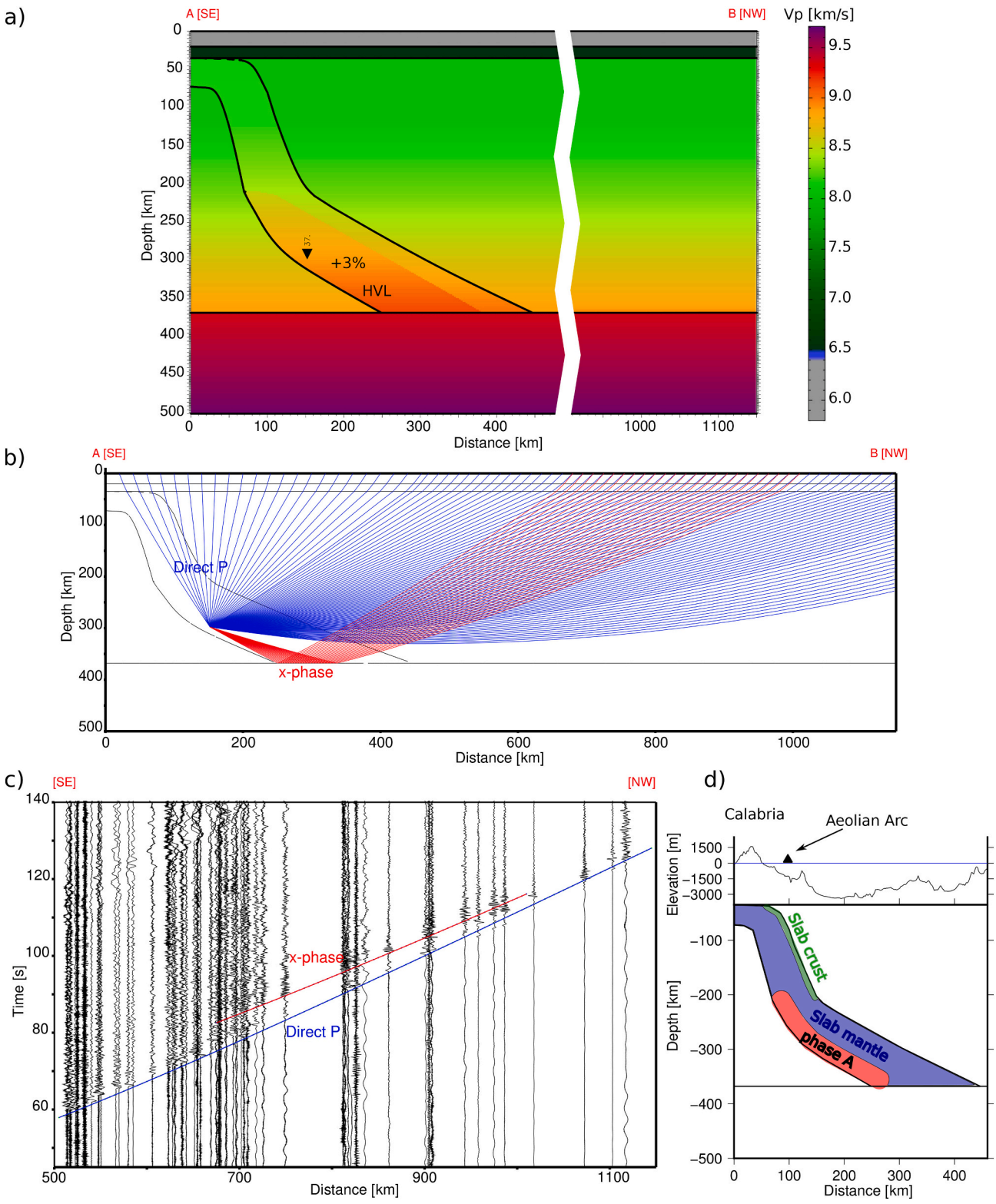

Fig. 10. (a) 2D velocity model, section trace in Fig. 2 (n.b. the section orientation is opposite of those in Fig. 3b-c to have increasing distances rightwards). The black triangle is the 2011 earthquake (N. 37) with x-phase; (b) Calculated ray paths for the earthquake N. 37; (c) calculated travel time curves on the observed record section of earthquake N. 37. The blue line shows the calculated direct P wave arrivals, and the red line is for the x-phase; (d) Sketch of the possible petrology and thickness of the HVL. (For interpretation of the references to colour in this figure legend, the reader is referred to the web version of this article.)

common finding from other subduction zones, although it is not excluded that it could be observed elsewhere. We also checked seismograms from Hellenic subduction and from some Vrancea intermediate-depth earthquakes without any interesting result. We noticed, anyway, that in Greece and in Romania there are no *x*-phase. Systematic research all around subduction zones will be part of the extension of this research in the future.

Finally, a comparison with laboratory experiments on mineral

transformations conducted at upper mantle conditions, provides a nice, elegant and simple explanation for the nature of our observations and allows us to make some important inferences on the origin of the *x*-phase.

We have shown that the earthquakes with the *x*-phase are located near the lower boundary of the seismic plate, probably in the uppermost mantle lithosphere of the subducted slab, between 215 to about 320 km of depth. The representing lithology that composes the lithospheric mantle at these depths is generally lherzolite and harzburgite (e.g., Hacker et al., 2003a). These rocks commonly enter into the subduction as locally hydrated, with water incorporated into OH-bearing minerals like antigorite serpentine and chlorite (see Fig. 5 in Hacker et al., 2003a). The slab deepening during subduction causes devolatilization reactions (e.g., Hacker et al., 2003a, 2003b) facilitating the embrittlement of these minerals. This process gives rise to earthquakes. When antigorite serpentine and chlorite react out at depth, not all the water escapes from the system and some can be still hold into a meta-stable mineral phase in the upper-mantle deep slab (e.g., Sclar et al., 1965; Cai et al., 2021). This mineral phase, which is a dense magnesium hydrated silicate, has been called in literature *phase A* (Sclar et al., 1965). Phase A is stable at higher pressure and temperature conditions and its importance is because it carries water deep into the Earth (Wunder and Schreyer, 1992; Fumagalli et al., 2001). Recent ultrasonic measurements of compressional waves on *phase A* in a cold subduction show an increase of *P*-velocities to the level introduced in the HVL model (Cai et al., 2021) and at depths from about 200 km and down. In addition, these depths are consistent with the range where we model the HVL in the Tyrrhenian subduction. Therefore, we interpret the HVL as related to the presence of the dense hydrous magnesium silicate *phase A*, formed after antigorite breakdown as inferred from laboratory experiments and predicted by phase equilibria in cold subduction zones (van Keken et al., 2011; Cai et al., 2021), as the Tyrrhenian subduction seems to be. This is the first direct seismological observation of the phase A in the subduction process.

CRediT authorship contribution statement

Teresa Ninivaggi: Conceptualization, Data curation, Investigation, Methodology, Software, Visualization. **Giulio Selvaggi:** Conceptualization, Methodology, Supervision, Data curation, Investigation, Writing – original draft. **Salvatore Mazza:** Conceptualization, Methodology, Software, Supervision, Writing – review & editing. **Marilena Filippucci:** Writing – review & editing, Conceptualization. **Fabrizio Tursi:** Conceptualization, Writing – review & editing. **Wojciech Czuba:** Software, Writing – review & editing.

Declaration of Competing Interest

The authors declare that they have no known competing financial interests or personal relationships that could have appeared to influence the work reported in this paper.

Data availability

For the creation of this manuscript the data were extracted from the following archives. Earthquakes data are from the Italian Seismological Instrumental and Parametric Database (ISIDe Working Group, 2007). Waveforms are extracted from the European Integrated Data Archive (EIDA, http://eida.ingv.it/) Infrastructure within the Observatories & Research Facilities for European Seismology (ORFEUS) and Federation of Digital Seismograph Networks (FDSN) and from the Incorporated Research Institutions for Seismology Data Management Centre (downloaded through the IRIS Web Services, https://service.iris.edu/). Most of the data are from the networks having the identifiers: IV, MN, NI, SI, SL, CH, GU, OE (Istituto Nazionale di Geofisica e Vulcanologia (INGV), 2005; MedNet Project Partner Institutions, 1990; OGS (Istituto Nazionale di Oceanografia e di Geofisica Sperimentale) and University of Trieste, 2002; Slovenian Environment Agency, 1990; Swiss Seismological Service (SED) At ETH Zurich, 1983; University of Genoa, 1967; ZAMG - Zentralanstalt für Meterologie und Geodynamik, 1987).

Acknowledgments

This work has been funded by INGV internal funding (Bando Ricerca Libera 2019) and supported by a subsidy from the Polish Ministry of Education and Science for the Institute of Geophysics, Polish Academy of Sciences.

Figures were made using the SAC software (Goldstein et al., 2003; Goldstein and Snoke, 2005) the Generic Mapping Tools (GMT), version 5 (Wessel et al., 2013) available at https://www.genericmapping-tools.org and the Obspy tool (Beyreuther et al., 2010).

We thank Prof. Johannes Schweitzer for his insightful comments and advice in the first stage of the work.

Appendix A. Supplementary data

Supplementary data to this article can be found online at https://doi.org/10.1016/j.tecto.2023.229919.

References

Abers, G.A., 2000. Hydrated subducted crust at 100–250 km depth. Earth Planet. Sci. Lett. 176 (3–4), 323–330. https://doi.org/10.1016/S0012-821X(00)00007-8.

Abers, G.A., 2005. Seismic low-velocity layer at the top of subducting slabs: observations, predictions, and systematics. Phys. Earth Planet. Inter. 149 (1–2), 7–29. https://doi.org/10.1016/j.pepi.2004.10.002.

Amato, A., Alessandrini, B., Cimini, G., Frepoli, A., Selvaggi, G., 1993. Active and remnant subducted slabs beneath Italy: evidence from seismic tomography and seismicity. Ann. Geophys. 36 (2) https://doi.org/10.4401/ag-4272.

Anderson, H., Jackson, J., 1987. Active tectonics of the Adriatic region. Geophys. J. R. Astron. Soc. 91, 937–983.

Beyreuther, M., Barsch, R., Krischer, L., Megies, T., Behr, Y., Wassermann, J., 2010. ObsPy: A Python toolbox for seismology SRL, 81 (3), 530–533. https://doi.org/10.1785/gssrl.81.3.530.

Cai, N., Qi, X., Chen, T., Wang, S., Yu, T., Wang, Y., et al., 2021. Enhanced visibility of subduction slabs by the formation of dense hydrous phase A. Geophys. Res. Lett. 48 (19), 1–10. https://doi.org/10.1029/2021GL095487.

Červený, V., Pšenčík, I., 1984. SEIS83-Numerical modelling of seismic wave fields in 2-D laterally varying layered structures by the ray method. In: Engdahl, E.R. (Ed.), Documentation of Earthquake Algorithms, Report SE-35. World Data Center A for Solid Earth Geophysics, Boulder, pp. 36–40.

Červený, V., Molotkov, I.A., Pšenčík, I., 1977. Ray method in seismology. Charles Univ. Press, Praha.

Chiarabba, C., De Gori, P., Speranza, F., 2008. The southern Tyrrhenian subduction zone: deep geometry, magmatism and Plio-Pleistocene evolution. Earth Planet. Sci. Lett. 268 (3–4), 408–423. https://doi.org/10.1016/j.epsl.2008.01.036.

Cimini, G.B., Marchetti, A., 2006. Deep structure of peninsular Italy from seismic tomography and subcrustal seismicity. Ann. Geophys. 49 (1), 331–345.

Collier, J.D., Helffrich, G.R., Wood, B.J., 2001. Seismic discontinuities and subduction zones. Phys. Earth Planet. Inter. 127 (1–4), 35–49. https://doi.org/10.1016/S0031-9201(01)00220-5.

D'Agostino, N., D'Anastasio, E., Gervasi, A., Guerra, I., Nedimović, M.R., Seeber, L., Steckler, M., 2011. Forearc extension and slow rollback of the Calabrian Arc from GPS measurements. Geophys. Res. Lett. 38, L17304. https://doi.org/10.1029/2011GL048270.

Essen, K., Braatz, M., Ceranna, L., Friederich, W., Meier, T., 2009. Numerical modelling of seismic wave propagation along the plate contact of the Hellenic Subduction Zone-the influence of a deep subduction channel. Geophys. J. Int. 179 (3), 1737–1756. https://doi.org/10.1111/j.1365-246X.2009.04369.x.

European Integrated Data Archive, 2023. http://eida.ingv.it/ (accessed 31 October 2021).

Faccenna, C., Becker, T.W., Lucente, F.P., Jolivet, L., Rossetti, F., 2001. History of subduction and back-arc extension in the Central Mediterranean. Geophys. J. Int. 145, 809–820. https://doi.org/10.1046/j.0956-540x.2001.01435.x.

Frepoli, A., Selvaggi, G., Chiarabba, C., Amato, A., 1996. State of stress in the Southern Tyrrhenian subduction zone from fault-plane solutions. Geophys. J. Int. 125 (3), 879–891. https://doi.org/10.1111/j.1365-246X.1996.tb06031.x.

Fukao, Y., Kanjo, K., Nakamura, I., 1978. Deep seismic zone as an upper mantle reflector of body waves. Nature 272, 606–608. https://doi.org/10.1038/272606a0.

Fumagalli, P., Stixrude, L., Poli, S., Snyder, D., 2001. The 10Å phase: a high-pressure expandable sheet silicate stable during subduction of hydrated lithosphere. Earth Planet. Sci. Lett. 186 (2), 125–141. https://doi.org/10.1016/S0012-821X(01)002382.

Furumura, T., Kennett, B.L.N., 2005. Subduction zone guided waves and the heterogeneity structure of the subducted plate: Intensity anomalies in northern Japan. J. Geophys. Res. 110, B10302. https://doi.org/10.1029/2004JB003486.
Furumura, T., Kennett, B.L.N., 2021. Azimuthal variation of lithospheric heterogeneity in the Northwest Pacific inferred from Po/So propagation characteristics and anomalously large ground motion of deep in-slab earthquakes. J. Geophys. Res. Solid Earth 126 (5), e2021JB021717. https://doi.org/10.1029/2021JB021717.
Furumura, T., Kennett, B.L.N., Padhy, S., 2016. Enhanced waveguide effect for deep-focus earthquakes in the subducting Pacific slab produced by a metastable olivine wedge. J. Geophys. Res. Solid Earth 121, 6779–6796. https://doi.org/10.1002/2016JB013300.
Goldstein, P., Snoke, A., 2005. SAC Availability for the IRIS Community. Incorporated Institutions for Seismology Data Management Center Electronic Newsletter.
Goldstein, P., Dodge, D., Firpo, M., Minner, Lee, 2003. SAC2000: Signal processing and analysis tools for seismologists and engineers. In: Lee, W.H.K., Kanamori, H., Jennings, P.C., Kisslinger, C. (Eds.), Invited contribution to "The IASPEI International Handbook of Earthquake and Engineering Seismology". Academic Press, London.
Hacker, B.R., Abers, G.A., Peacock, S.M., 2003a. Subduction factory 1. Theoretical mineralogy, densities, seismic wave speeds, and H_2O contents. J. Geophys. Res. Solid Earth 108 (B1), 1–26. https://doi.org/10.1029/2001jb001127.
Hacker, B.R., Peacock, S.M., Abers, G.A., Holloway, S.D., 2003b. Subduction factory 2. Are intermediate-depth earthquakes in subducting slabs linked to metamorphic dehydration reactions? J. Geophys. Res. Solid Earth 108 (B1). https://doi.org/10.1029/2001jb001129.
Hasegawa, A., Umino, N., Takagi, A., 1978. Double-planed structure of the deep seismic zone in the northeastern Japan arc. Tectonophysics 47 (1–2), 43–58.
Hori, S., 1990. Seismic waves guided by untransformed oceanic crust subducting into the mantle: the case of the Kanto district, central Japan. Tectonophysics 176 (3–4), 355–376.
Incorporated Research Institutions for Seismology Data Management Centre, 2023. https://service.iris.edu/ (accessed 31 October 2021).
ISIDe Working Group, 2007. Italian Seismological Instrumental and Parametric Database (ISIDe) [Dataset]. Istituto Nazionale di Geofisica e Vulcanologia (INGV). https://doi.org/10.13127/ISIDE.
Istituto Nazionale di Geofisica e Vulcanologia (INGV), 2005. Rete Sismica Nazionale (RSN) [Dataset]. Istituto Nazionale di Geofisica e Vulcanologia (INGV). https://doi.org/10.13127/SD/X0FXNH7QFY.
Kennett, B.L.N., Engdahl, E.R., 1991. Traveltimes for global earthquake location and phase identification. Geophys. J. Int. 105, 429–465. https://doi.org/10.1111/j.1365-246X.1991.tb06724.x.
Kennett, B.L.N., Furumura, T., 2013. High-frequency Po/So guided waves in the oceanic lithosphere: I-long-distance propagation. Geophys. J. Int. 195, 1862–1877. https://doi.org/10.1093/gji/ggt344.
Kennett, B.L.N., Furumura, T., 2015. Toward the reconciliation of seismological and petrological perspectives on oceanic lithosphere heterogeneity. Geochem. Geophys. Geosyst. 16, 3129–3141. https://doi.org/10.1002/2015GC006017.
Komminaho, K., 1998. Software Manual for Programs MODEL and XRAYS—a Graphical Interface for SEIS83 program package, 20. University of Oulu, Dep. of Geophys., Rep, p. 31.
Latorre, D., Di Stefano, R., Castello, B., Michele, M., Chiaraluce, L., 2023. An updated view of the Italian seismicity from probabilistic location in 3D velocity models: the 1981–2018 Italian catalog of absolute earthquake locations (CLASS). Tectonophysics 846, 229664. https://doi.org/10.1016/j.tecto.2022.229664.
Lin, C.H., 2016. Evidence for a magma reservoir beneath the Taipei metropolis of Taiwan from both *S*-wave shadows and *P*-wave delays. Sci. Rep. 6, 39500. https://doi.org/10.1038/srep39500.
Lin, C.H., Lai, Y.C., Shih, M.H., Pu, H.C., Lee, S.J., 2018. Seismic detection of a magma reservoir beneath Turtle Island of Taiwan by S-Wave shadows and reflections. Sci. Rep. 8 (1), 16401. https://doi.org/10.1038/s41598-018-34596-0.
Lucente, F.P., Chiarabba, C., Cimini, G.B., Giardini, D., 1999. Tomographic constraints on the geodynamic evolution of the Italian region. J. Geophys. Res. Solid Earth 104 (B9), 20307–20327. https://doi.org/10.1029/1999JB900147.
Martin, S., Rietbrock, A., 2006. Guided waves at subduction zones: dependencies on slab geometry, receiver locations and earthquake sources. Geophys. J. Int. 167, 693–704. https://doi.org/10.1111/j.1365-246X.2006.02963.x.
Martin, S., Rietbrock, A., Haberland, C., Asch, G., 2003. Guided waves propagating in subducted oceanic crust. J. Geophys. Res. 108 (B11), 2536. https://doi.org/10.1029/2003JB002450.
Matsuzawa, T., Umino, N., Hasegawa, A., Takagi, A., 1986. Upper mantle velocity structure estimated from PS-converted wave beneath the north-eastern Japan Arc. Geophys. J. Int. 86 (3), 767–787. https://doi.org/10.1111/j.1365-246X.1986.tb00659.x.
MedNet Project Partner Institutions, 1990, January 1. Mediterranean Very Broadband Seismographic Network (MedNet) [Dataset]. Istituto Nazionale di Geofisica e Vulcanologia (INGV). 10.13127/SD/FBBBTDTD6Q.
Murphy, J.R., Barker, B.W., 2006. Improved focal-depth determination through automated identification of the seismic depth phases pP and sP. Bull. Seismol. Soc. Am. 96 (4A), 1213–1229. https://doi.org/10.1785/0120050259.
Obara, K., Sato, H., 1988. Existence of an S wave reflector near the upper plane of the double seismic zone beneath the Southern Kanto District, Japan. J. Geophys. Res. 93 (B12), 15037–15045. https://doi.org/10.1029/JB093iB12p15037.
OGS (Istituto Nazionale di Oceanografia e di Geofisica Sperimentale) and University of Trieste, 2002. North-East Italy Broadband Network [Dataset]. International Federation of Digital Seismograph Networks. https://doi.org/10.7914/SN/NI.
Ohmi, S., Hori, S., 2000. Seismic wave conversion near the upper boundary of the Pacific plate beneath the Kanto district, Japan. Geophys. J. Intern. 141 (1), 136–148. https://doi.org/10.1046/j.1365-246X.2000.00086.x.
Pino, N.A., Helmberger, D.V., 1997. Upper mantle compressional velocity structure beneath the West Mediterranean Basin. J. Geophys. Res. 102 (B2), 2953–2967. https://doi.org/10.1029/96JB03461.
Ritsema, A.R., 1972. Deep earthquakes of the Tyrrhenian Sea. Geol. Mijnb. 51 (5), 541–545.
Scarfì, L., Barberi, G., Barreca, G., Cannavò, F., Koulakov, I., Patanè, D., 2018. Slab narrowing in the Central Mediterranean: the Calabro-Ionian subduction zone as imaged by high resolution seismic tomography. Sci. Rep. 8 (1), 1–12. https://doi.org/10.1038/s41598-018-23543-8.
Sclar, C.B., Carrison, L.C., Schwartz, C.M., 1965. High-pressure synthesis and stability of a new hydronium-bearing layer silicate in the system $MgO–SiO_2–H_2O$. Trans. Am. Geophys. Union 46, 184.
Selvaggi, G., 2001. Strain pattern of the Southern Tyrrhenian slab from moment tensors of deep earthquakes: implications on the down-dip velocity. Ann. Geophys. 44 (1) https://doi.org/10.4401/ag-3613.
Selvaggi, G., Chiarabba, C., 1995. Seismicity and P-wave velocity image of the Southern Tyrrhenian subduction zone. Geophys. J. Int. 121 (3), 818–826. https://doi.org/10.1111/j.1365-246X.1995.tb06441.x.
Slovenian Environment Agency, 1990. Seismic Network of the Republic of Slovenia [Dataset]. International Federation of Digital Seismograph Networks. https://doi.org/10.7914/SN/SL.
Spakman, W., van der Lee, S., van der Hilst, R., 1993. Travel-time tomography of the European-Mediterranean mantle down to 1400 km. Phys. Earth Planet. Inter. 79 (1–2), 3–74. https://doi.org/10.1016/0031-9201(93)90142-V.
Sun, D., Miller, M.S., Agostinetti, N.P., Asimow, P.D., Li, D., 2014. High frequency seismic waves and slab structures beneath Italy. Earth Planet. Sci. Lett. 391, 212–223. https://doi.org/10.1016/j.epsl.2014.01.034.
Swiss Seismological Service (SED) At ETH Zurich, 1983. National Seismic Networks of Switzerland [Dataset]. ETH Zürich. https://doi.org/10.12686/SED/NETWORKS/CH.
University of Genoa, 1967. Regional Seismic Network of North Western Italy [Dataset]. International Federation of Digital Seismograph Networks. https://doi.org/10.7914/SN/GU.
van Keken, P.E., Hacker, B.R., Syracuse, E.M., Abers, G.A., 2011. Subduction factory: 4. Depth-dependent flux of H2O from subducting slabs worldwide. J. Geophys. Res. 116, B01401. https://doi.org/10.1029/2010JB007922.
Wessel, P., Smith, W.H., Scharroo, R., Luis, J., Wobbe, F., 2013. Generic mapping tools: improved version released. EOS Trans. Am. Geophys. Union 94 (45), 409–410. https://doi.org/10.1002/2013EO45000.
Wunder, B., Schreyer, W., 1992. Metastability of the 10-Å phase in the system MgO-SiO2-H2O (MSH). what about hydrous MSH phases in subduction zones? J. Petrol. 33 (4), 877–889. https://doi.org/10.1093/petrology/33.4.877.
ZAMG - Zentralanstalt für Meterologie und Geodynamik, 1987. Austrian Seismic Network [Dataset]. International Federation of Digital Seismograph Networks. https://doi.org/10.7914/SN/OE.
Zelt, C.A., 1994. ZPLOT-An Interactive Plotting and Picking Program for Seismic Data. Bullard Lab., University of Cambridge, Cambridge UK.
Zhao, C.A., 2019. Importance of later phases in seismic tomography. Phys. Earth Planet. Inter. 296, 106314 https://doi.org/10.1016/j.pepi.2019.106314.
Zhao, D., Matsuzawa, T., Hasegawa, A., 1997. Morphology of the subducting slab boundary in the northeastern Japan arc. Phys. Earth Planet. Inter. 102 (1–2), 89–104. https://doi.org/10.1016/S0031-9201(96)03258-X.